Article

A physicochemical-sensing electronic skin for stress response monitoring

Changhao Xu [1,5], Yu Song [1,5], Juliane R. Sempionatto [1,5], Samuel A. Solomon[1,5], You Yu[1], Hnin Y. Y. Nyein[2], Roland Yingjie Tay [1], Jiahong Li[1], Wenzheng Heng[1], Jihong Min [1], Alison Lao [1], Tzung K. Hsiai[3], Jennifer A. Sumner [4] & Wei Gao [1] ✉

Approaches to quantify stress responses typically rely on subjective surveys and questionnaires. Wearable sensors can potentially be used to continuously monitor stress-relevant biomarkers. However, the biological stress response is spread across the nervous, endocrine and immune systems, and the capabilities of current sensors are not sufficient for condition-specific stress response evaluation. Here we report an electronic skin for stress response assessment that non-invasively monitors three vital signs (pulse waveform, galvanic skin response and skin temperature) and six molecular biomarkers in human sweat (glucose, lactate, uric acid, sodium ions, potassium ions and ammonium). We develop a general approach to prepare electrochemical sensors that relies on analogous composite materials for stabilizing and conserving sensor interfaces. The resulting sensors offer long-term sweat biomarker analysis of more than 100 h with high stability. We show that the electronic skin can provide continuous multimodal physicochemical monitoring over a 24-hour period and during different daily activities. With the help of a machine learning pipeline, we also show that the platform can differentiate three stressors with an accuracy of 98.0% and quantify psychological stress responses with a confidence level of 98.7%.

Stress is a process triggered by demanding physical or psychological events and may cause anxiety as a prototypical psychological response. Although acute stress responses in healthy individuals can be adaptive and manageable, persistent experiences of stress can have deleterious effects on mental and physical health[1,2], and many mechanisms behind the stress response are yet unknown[3,4] (Supplementary Note 1). In the United States alone, more than 50 million adults suffer from depression, and after the onset of the COVID-19 pandemic, the number of people suffering from mental disorders has drastically risen, causing a heavy burden on the healthcare system[5,6]. Elevated levels of stress and anxiety also pose a large burden to high-demand occupation workers[7] such as

athletes[8], soldiers[9], first responders[10] and aviation personnel[11], potentially interfering with their cognitive performance and decision-making process[12]. In response to these effects, understanding and evaluating the stress response has become a cornerstone of clinical healthcare. However, current gold standards for clinical stress response assessments rely on surveys and performance evaluations, which can be highly subjective[13–15]. Thus, there is a need to develop a more efficient and effective stress assessment tool that is not characterized by these limitations[16,17].

Non-invasive biomarkers are potentially a reliable alternative for monitoring the stress response because of the interdependencies

[1]Andrew and Peggy Cherng Department of Medical Engineering, Division of Engineering and Applied Science, California Institute of Technology, Pasadena, CA, USA. [2]Department of Chemical and Biological Engineering, Hong Kong University of Science and Technology, Hong Kong, China. [3]Division of Cardiology, David Geffen School of Medicine, University of California, Los Angeles, CA, USA. [4]Department of Psychology, University of California, Los Angeles, CA, USA. [5]These authors contributed equally: Changhao Xu, Yu Song, Juliane R. Sempionatto, Samuel A. Solomon. ✉e-mail: weigao@caltech.edu
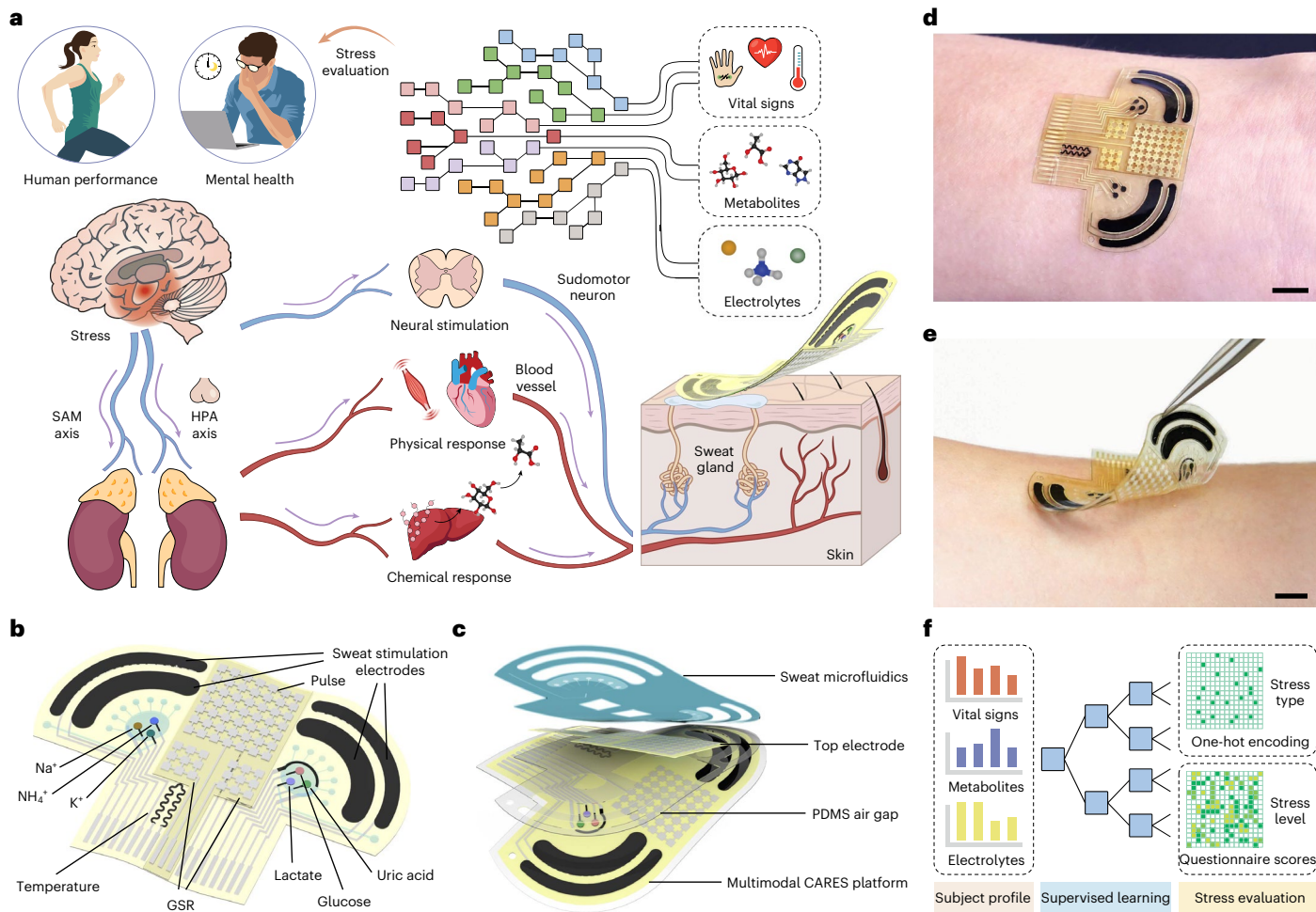
Fig. 1 | CARES for stress response monitoring. a, Illustration of the CARES that continuously monitors multimodal physiological and biochemical responses from skin and performs artificial-intelligence-powered stress assessment. **b**, Schematic of the flexible CARES sensor patch and main functionalities: vital sign monitoring, sweat stimulation and sampling and key metabolite and electrolyte detection. **c**, Schematic of layered structure of the CARES that assembles the sensor and microfluidics module. **d**,**e**, Optical images of a CARES attached to the skin of a human subject (**d**) and the soft electronic-skin interface (**e**). Scale bars, 1 cm. **f**, ML pipeline for CARES-enabled stressor classification and stress/anxiety level assessment. SAM, sympathetic–adreno–medullar.

between biological and psychological stress. In particular, stress induces a complex biological response in the nervous, endocrine and immune systems (Fig. 1a)[18,19]. The perception of stress activates the hypothalamic–pituitary–adrenal (HPA) axis and sympathetic adrenal medullary axis from the hypothalamus in the brain. Acetylcholine in nerve fibres from both axes stimulates the adrenal gland, releasing stress hormones (for example, epinephrine, norepinephrine and cortisol) into the blood. Acetylcholine can also activate sudomotor neurons connected to sweat glands that release ion-rich fluids. This sympathetic activity can be indirectly measured through the galvanic skin response (GSR) and sweat electrolyte levels[20]. The released stress hormones inhibit insulin production, affecting the synthesis of metabolites such as glucose, lactate and uric acid (UA), as well as narrow arteries, boosting cardiac activities. By monitoring these stress-relevant biomarkers, it is possible to develop a comprehensive and objective health profile relating biophysical and biochemical signals to dynamic stress response monitoring[21–23].

Recent advances in wearable sensors have enabled real-time and continuous monitoring of physical vital signs[24–28]. Through in situ human sweat analysis, wearable biosensors can provide insightful information about an individual's health at the molecular level[29–32]. However, various challenges remain to be addressed before such sensors can be of use in clinical applications: a limited set of physical signals

are not sufficient for condition-specific assessment of psychological and physiological stress[33]; existing wearable biochemical sensors suffer from poor operational stability in biofluids, which precludes reliable long-term continuous monitoring[34]; access to human sweat usually requires physical activity that can affect an individual's stress; and despite recent progress on stress hormone analysis, continuous monitoring of sweat stress hormones at physiologically relevant levels using wearable sensors has not yet been achieved because of the hormones' extremely low concentrations[35–37]. Therefore, although understanding and monitoring the endocrine response to stress is a promising approach, it is still underdeveloped.

In this Article, we report a consolidated artificial-intelligence-reinforced electronic skin (CARES) with robust long-term sensing capabilities for stress response monitoring (Fig. 1a). Fabricated using a scalable inkjet-printing approach, the wearable device is capable of multiplexed, non-invasive monitoring of key stress-related physiological signals (pulse waveform, GSR and skin temperature), sweat metabolites (glucose, lactate and UA) and electrolytes (Na^+, K^+ and NH_4^+) during daily activities (Fig. 1b,c). Through the integration of a miniaturized iontophoresis (IP) module, sweat can be induced autonomously at rest without the need for vigorous exercise.

We develop a general approach to prepare highly stable and sensitive electrochemical biosensors, which uses analogous composite

materials for stabilizing and conserving sensor interfaces. The resulting biochemical sensors offer long-term stability of more than 100 h of continuous operation with minimal signal drifts (amperometric signals decaying less than 0.07% per hour and potentiometric signals drift less than 0.04 mV per hour).

Built on an ultrathin flexible polyimide (PI) substrate (4 μm) for flexibility and robustness as well as integrated with microfluidics, the CARES device conformally laminates on the wrist for reliable and robust sensing (Fig. 1d,e). This allows for 24-hour continuous monitoring of daily activities, yielding greater insight into how these signals vary throughout the day. With a machine learning (ML) pipeline incorporating previously inaccessible multimodal data (Fig. 1f), we show that the physicochemical sensor data obtained by the wearable technology can be used to classify responses to stressors at high accuracies and predict state anxiety levels (a key psychological response to stress) with high reliability.

The CARES platform

The CARES platform consists of a multilayered sensor patch and a skin-interfaced laser-engraved microfluidic module (Fig. 1d,e). The sensor patch contains carbachol hydrogel-loaded sweat-stimulation electrodes, three enzymatic biosensors, three ion-selective sensors (ISEs), a capacitive pulse sensor, a resistive GSR sensor and a skin temperature sensor. The platform can be mass-fabricated through serial inkjet printing of silver and carbon as the interconnects and electrodes for the top and bottom layers (Supplementary Fig. 1). A middle polydimethylsiloxane (PDMS)-based airgap layer was spin-coated between the top and bottom layers, as the soft PDMS facilitates pulse pressure sensitivity and sweat reservoir collection. The microfluidic module was assembled in a sandwiched structure (PDMS/polyethylene terephthalate/medical tape) and contains two separate reservoirs (Supplementary Figs. 2 and 3) that enable fresh sweat sampling and rapid refreshing for accurate sweat analysis with high temporal resolution. Carbachol was used for sweat induction as it enables long-lasting sudomotor axon reflex sweat secretion from the surrounding sweat glands owing to its nicotinic effects[38]. In this work, six molecular biomarkers (glucose, lactate, UA, Na^+, K^+ and NH_4^+) were selected as the detection targets because of their strong associations with stress responses (Supplementary Note 2)[39–43]. Together with laser-patterned microfluidics, the CARES device can be attached to the subject's wrist comfortably and performs multiplexed metabolic sensing in situ.

Wearable sensors for long-term continuous operation

Several electrochemical sensing strategies based on enzymes[29], ionophores[44], molecularly imprinted polymers[30], aptamers[45] and antibodies[46] are reported, and the majority of existing wearable chemical sensors are primarily based on amperometric enzymatic sensors or potentiometric ISEs as these sensors can offer real-time continuous monitoring with high temporal resolution. However, one main bottleneck for the practical applications of these sensors is their limited operation lifetime and long-term stability during continuous wearable sensing. Large sensor drifts are evident when they are used in body fluids, which substantially hinders the long-term continuous usability of wearable chemical sensors.

Most wearable enzymatic biosensors are based on Prussian blue (PB), which serves as an efficient electron-transfer mediator with a low redox potential of around 0 V. However, PB-based biosensors suffer from poor stability during long-term use in biofluids because PB degrades in neutral and alkaline solutions as the hydroxide ions (OH^-), a product of H_2O_2 reduction, can break the Fe–(CN)–Fe bond (Supplementary Note 3). To stabilize PB while retaining its catalytic activity, we use a PB-analogue nickel hexacyanoferrate (NiHCF) with a similar zeolitic crystal structure that is catalytically inactive but forms a stabilized solid solution composite, protecting the PB sensor

interface (Fig. 2a). Additionally, the enzymes were protected in a glutaraldehyde-crosslinked bovine serum albumin (BSA) matrix. To fabricate enzymatic sensors, gold nanoparticles were electrodeposited onto an inkjet-printed inert carbon electrode to provide a high electroactive area for sensitive electrochemical sensing followed by PB–NiHCF deposition. Scanning transmission electron microscopy (STEM) and energy dispersive spectroscopy (EDS) analyses (Fig. 2b and Supplementary Fig. 4) indicate that NiHCF forms a thin protective layer on PB with an obscure boundary. Our electrochemical characterizations confirmed that compared to PB–which suffered from rapid degradation during electrochemical measurement–and other transition metal hexacyanoferrates (PB–CoHCF and PB–CuHCF), PB–NiHCF could withstand pH corrosion and maintain the most consistent electrochemical catalytic activity (Supplementary Figs. 5–7). This could be attributed to two mechanisms (Supplementary Note 3): (1) nickel is inert compared with iron and can withstand OH^- group corrosion (Supplementary Fig. 8), and (2) the Ni ion has a smaller ionic radius than other transitional metal ions (such as Co and Cu ions), which is better able to withstand ion insertion (Supplementary Fig. 9). Both mechanisms were further supported with scanning electron microscope characterizations of the electrodes (Supplementary Fig. 10) and inductively coupled plasma–mass spectrometry analysis of the dissolved Fe^{2+} from the electrodes (Supplementary Fig. 11) before and after electrochemical tests. These results indicated that PB dissolved after tests under different pHs and repeated cyclic voltammetry scans, whereas NiHCF did not show any substantial degradation and maintained the highest stability among the transition metal hexacyanoferrates for PB stabilization.

Highly stable, continuous and selective monitoring of sweat glucose, lactate and UA was realized amperometrically, and a linear response between current output and target concentrations was obtained for all three sensors in physiologically relevant concentration ranges over a 25 h evaluation period (Fig. 2c). The sensitivities for glucose, lactate and UA sensors were 33.65 nA μM^{-1} cm^{-2}, 185.56 nA mM^{-1} cm^{-2} and 26.36 nA μM^{-1} cm^{-2}, respectively. These sensors also showed long-term stability of more than 100 h of continuous operation in phosphate-buffered saline (PBS) solutions and untreated human sweat samples, which greatly exceeded that obtained with previous widely adopted wearable sweat sensors (Supplementary Figs. 12 and 13 and Table 1). Note that as sweat lactate is present in high concentrations (up to 60 mM), a further diffusion-limited polyvinyl chloride (PVC)/bis(2-ethylhexyl) sebacate (DOS) membrane was introduced on top of the enzyme film to achieve a wide linear range while maintaining high sensor stability (Supplementary Fig. 14).

Existing wearable ISEs are based on PVC/DOS membranes and are plagued with a potential drift of typically ~2 mV per hour over time, which is attributed to ionophore leaching and water formation below the ion-selective membrane[47]. To address this issue during long-term operation, we adopted another analogous composite materials design strategy by introducing polystyrene-block-poly (ethylene butylene)-block-polystyrene (SEBS) into the PVC system; it shares a similar long-chain structure but holds more methyl and phenyl groups at the sensor interface to promote hydrophobicity and mechanical strength (Fig. 2d). High hydrophobicity suppresses ionophore leaching and prevents water layer formation at the interface. To fabricate ISEs, electrodes made from inkjet-printed carbon nanoparticles, which are inert but have a large surface area, were used without the need to deposit further ion-charge transducer materials. Ion-selective membranes based on the PVC–SEBS matrix were drop-casted onto the carbon electrode, and the SEBS to PVC ratio was evaluated to identify the optimal stability (Fig. 2e, Supplementary Note 4). The optimized ISEs obtained prolonged stability of 100 h of continuous operation in both standard solutions and human sweat samples, with the potential value decaying less than 0.04 mV per hour (Supplementary Figs. 15 and 16 and Table 2). A logarithmic–linear relationship between the potentiometric output of Na^+, K^+ and NH_4^+ with near-Nernstian sensitivities of
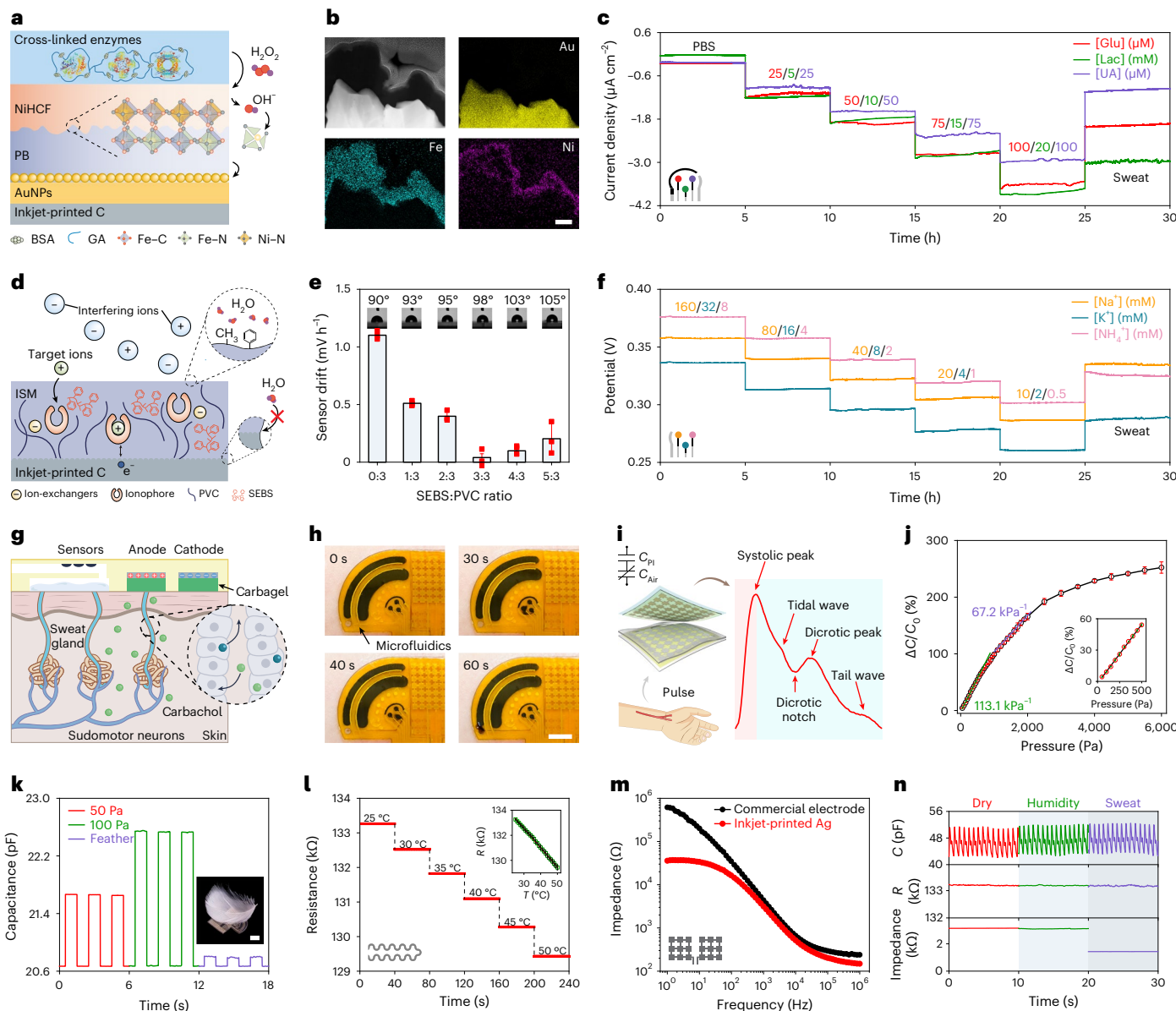
Fig. 2 | Design and characterization of highly robust multimodal sensors.
a, Mechanism of enzymatic metabolite sensors. **b**, Cross-sectional STEM and EDS images of the PB–NiHCF interface. Scale bar, 100 nm. **c**, Operational long-term stability of enzymatic glucose, lactate and UA sensors in PBS and sweat samples for 30 h. **d**, Mechanism of ISEs. **e**, SEBS to PVC ratios in regards to sensor stability. Insets, contact angle measurements for different SEBS ratios. Data are presented as mean ± s.d. (n = 3 sensors). **f**, Operational long-term stability of ion-selective Na$^+$, K$^+$ and NH$_4^+$ sensors in standard solutions and sweat samples for 30 h. **g**,**h**, Schematic (**g**) and on-body evaluation (**h**) of the microfluidic IP module for autonomous sweat induction and sampling at rest. Timestamps in **h** represent the period after a 5 min IP session. **i**, Schematic of the pressure sensor and a pulse waveform measured at the wrist. C_{PI}, capacitance of the polyimide; C_{Air},

capacitance of the airgap. **j**, Pressure versus capacitance (C) characterizations of the pressure sensor, where C_0 is flat-state C. Data are presented as mean ± s.d. (n = 3 sensors). **k**, Repetitive response of the pressure sensor on small pressure loads. Inset, a goose feather placed on a sensor. Scale bar, 1 cm. **l**, Response of the temperature (T) sensor in the physiological temperature range. **m**, Impedance of the skin–electrode interface measured with inkjet-printed Ag electrodes and commercial electrodes for GSR monitoring. **n**, Performance of encapsulated pulse, T and GSR sensors under environmental humidity and body sweat test. All error bars represent the s.d. from three sensors. AuNPs, gold nanoparticles; carbagel, carbachol hydrogel; GA, glutaraldehyde; Glu, glucose; Lac, lactate; ISM, ion-selective membrane; R, resistance.

58.9, 60.6 and 61.2 mV per decade, respectively, were identified during a 25 h prolonged sensor evaluation in physiologically relevant ranges (Fig. 2f and Supplementary Fig. 17).

With an analogous composite materials' approach, our sensors demonstrated high reproducibility (Supplementary Fig. 18), selectivity (Supplementary Fig. 19) and long-term continuous operation stability in both standard solutions and untreated human sweat over several days (Supplementary Figs. 12, 13, 15 and 16). Such sensor performance, to the best of our knowledge, was among the best in wearable sweat

sensing (Supplementary Tables 1 and 2). The low-cost, mass-producible sensor patch is designed to be disposable after use: the anticipated wearable use time for each patch is 24–48 h, and users can easily replace the sensor patch. Thus, our sensors can provide a stable response for longer than the expected wearable use time. The general material strategy demonstrated here, based on electrodes prepared by inkjet printing, can be applicable to electrodes manufactured using other scalable technologies, including laser engraving and thin-film evaporation (Supplementary Fig. 20). In addition, the sensor preparation

approach here is not limited to the six sensors we proposed in this study; it can serve as a universal and readily reconfigurable method for other enzymatic and ionophore-based biosensors towards a broad range of practical applications.

To realize practical molecular biomarker monitoring without the need for vigorous exercise, miniaturized IP electrodes coated with carbachol hydrogels were incorporated into the CARES for autonomous, local sweat induction (Fig. 2g). Sweat can be continuously secreted from the surrounding glands over a prolonged period of time because of the nicotinic effects of carbachol (transdermally delivered for 5 min by means of a 50 µA current). Efficient sampling was obtained through custom-developed microfluidics for real-time bioanalysis with high temporal resolution (Fig. 2h and Supplementary Figs. 21 and 22 and Supplementary Video 1).

In addition to chemical sensors, the CARES also contains several physical sensors to monitor stress-related vital signs. We placed a capacitive pressure sensor above the radial artery for pulse waveform monitoring (Fig. 2i). Because of the soft PDMS-engraved airgap, the pressure sensor is highly sensitive to soft pressure loads (such as a feather), with an impressive sensitivity of 113.1% kPa^{-1} in the range of 0 to 500 Pa (Fig. 2j,k). The pressure sensor also displays highly robust performance and mechanical stability during a repetitive pressure-loading test involving 5,000 cycles, mimicking daily use on the skin (Supplementary Fig. 23). A printed resistive temperature sensor was integrated into the CARES for skin temperature recording in situ, with a sensitivity of around 0.115% °C^{-1} in physiological temperature ranges between 25 and 50 °C (Fig. 2l and Supplementary Fig. 24). Considering that temperature has a strong influence on enzymatic activities, the temperature information is used for calibrating the response of the three enzymatic biosensors to achieve highly accurate in situ metabolic analysis (Supplementary Figs. 25 and 26). Note that other environmental factors such as humidity showed minimal influence on the performance of our chemical sensors (Supplementary Fig. 27). Additionally, a pair of printed Ag electrodes was used as a GSR sensor, which demonstrated high conductivity compared with commercial gel electrodes (Fig. 2m). Because of the ultrathin flexible PI substrate and strong interfacial strength enabled by the medical adhesive, the CARES showed excellent skin contact and mechanical resilience against undesirable physical deformations during continuous operations (Supplementary Figs. 28 and 29). The impermeable PI packaging also eliminated the influence of humidity from environmental surroundings and sweat (Fig. 2n).

Continuous daily monitoring across various activities

Because of the excellent long-term stability of wearable sweat biosensors, the CARES enables long-term real-time continuous monitoring of physicochemical biomarkers. As illustrated in Fig. 3a, the CARES can successfully record dynamic changes in metabolites and vital signs over 24 h of activity involving casual and vigorous exercise, dietary intake, lab work, relaxing entertainment and sleep. Glucose and UA levels spiked after food intake, indicating rapidly increased metabolic activities. During vigorous exercise, substantial increases in vascular activity and skin electrolyte/conductivity were observed, and stable output for both metabolites and vital signs was detected during sleep at night. Such powerful capabilities of continuous multimodal monitoring will enable various personalized healthcare and human performance monitoring applications.

ML approach for stress evaluation

To evaluate the use of the CARES for stress response monitoring, controlled experiments were performed on ten healthy subjects using three different physiological and psychological stressors: a cold pressor test (CPT), a virtual reality (VR) challenge and intense exercise (Supplementary Note 5). The dynamic profiles of all individual sensors integrated in the CARES were collected during each study, as illustrated in Fig. 3b–d

and Supplementary Figs. 30–33. State anxiety levels, as measured by the State-Trait Anxiety Inventory Form Y (STAI-Y) questionnaire, with scores ranging between 10 and 40 points (10 indicating little to no anxiety)[48], were the psychological stress response measure for data training (Supplementary Note 6). The questionnaire was administered before and after each stressor to quantify the induced anxiety levels in a subject (Supplementary Fig. 34).

For each experiment, on-body chemical and physical data showed notable variations in response to each stressor. During the CPT experiment, subjects immersed one hand in ice water for 3 min. A natural reaction of vasoconstriction occurred, and the blood vessel constricted in response to cold temperatures[49]. As a result, immediate physiological responses including altered pulse waveform and elevated GSR were observed, consistent with previous reports on the variations of physiological signals with cold-stimulated stress response[50,51]. In addition, delayed mild fluctuations in metabolite concentrations of glucose, lactate and UA in some subjects were also observed. During the VR test, subjects wore an Oculus VR headset to play a rhythm game (Beat Saber) while the gaming screen was mirrored to a computer monitor with an audience, resulting in both physiological and social–evaluative psychological stress. We observed substantial differences in the pulse waveform and GSR amplitude during and after the stress stimulus, along with elevated glucose, lactate and UA levels minutes later[39–41]. During vigorous exercise, profound activation of the HPA axis led to dramatic changes of all physiological signals as well as sweat metabolites and electrolytes (for example, Na$^+$), in agreement with previous studies on exercise-induced stress response[42,52]. These results indicate that the CARES can reliably monitor stress-induced biological signals.

To quantify the stress-response-related features, data-driven stress and anxiety evaluations were performed after each experiment was complete: an ML pipeline was developed to extract features and deconvolute connections between physicochemical information and stressor types and state anxiety levels (Fig. 4a and Supplementary Note 7). We undertook this challenge using three separate ML analyses: stress detection versus relaxation, stressor classification and anxiety level evaluation, where we trained and tested each model across three experiments (VR, CPT, exercise) with all ten subjects for a total of 60,000 s of physiological CARES signals. All signals were calibrated and normalized to ensure that the features extracted after data preprocessing were stable against patch variations and any moderate motion artifacts (Supplementary Figs. 35–37, Note 8 and Table 3). Feature extraction was validated before ML analysis by projecting the multidimensional feature space into 2D space by means of t-distributed stochastic neighbour embedding[53], where data from stress/relaxation naturally formed distinctive clusters, indicating the discriminative power of the features (Fig. 4b, Supplementary Fig. 38a).

Different ML models were evaluated, and the trained boosting decision tree model Extreme Gradient Boosting (XGBoost) outperformed typical ML models, including linear and radial basis function support vector machines (SVMs), logistic and ridge regression and conventional decision trees (Fig. 4c). Combined with features extracted from both physiological and metabolic data, it was found that our XGBoost ML model could yield much higher accuracy, with stress response classification accuracy of 99.2% for stress/relaxation detection (Supplementary Fig. 38) and an accuracy of more than 98.0% for stressor classification, which to the best of our knowledge is the highest accuracy reported for stressor classification (Fig. 4d and Supplementary Table 4). Note that differentiating stressors has high importance, as each stressor carries varying physiological and psychological influences and could act as a risk factor for coping responses and cardiovascular diseases[54–56]. Distinguishing types of stressors has been recognized as a necessary condition for understanding the complex interrelationships among distinct stress experiences, as well as the collective effects of stress on mental health[57] (Supplementary Note 5). Moreover, the XGBoost ML model resulted in highly consistent overall
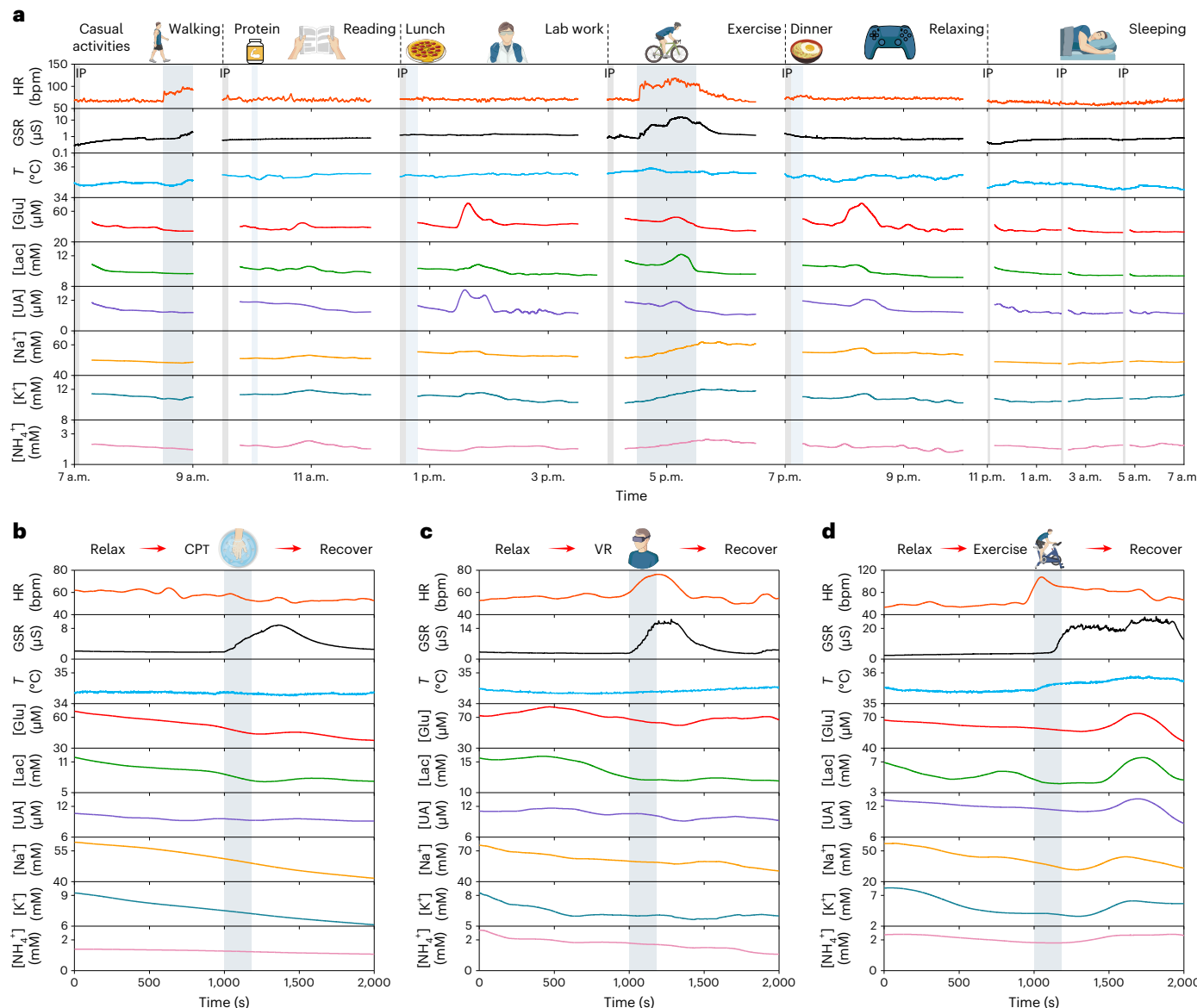
Fig. 3 | On-body evaluation of the CARES in daily activities and under various types of physiological and psychological stressors. a, Continuous 24 h multimodal monitoring during a subject's daily activities. **b–d**, Multimodal monitoring of a selected subject's stress response under three different stressors: a CPT challenge, during which the subject was asked to immerse one hand in ice water (**b**); a VR challenge, during which the subject was asked to play a VR rhythm game (**c**); and a cycling exercise test, during which the subject was asked to perform a maximum-load cycling challenge on a stationary exercise bike (**d**). HR, heart rate; bpm, beats per minute.

accuracies of more than 99.3% across different individuals (Fig. 4e and Supplementary Note 9).

The Pearson correlation coefficients between all sensors in the CARES show the interrelatedness between physiological and chemical biomarkers (Fig. 4f). The relatively homogeneous correlation shows the high independence of the extracted features. To evaluate each physicochemical sensor's contribution to the model, feature importance of each biomarker towards each stressor was evaluated using a Shapley additive explanation (SHAP) (Fig. 4g and Supplementary Fig. 39 and Note 9). Through SHAP analysis, the feature importance of GSR, pulse, glucose and Na^+ indicates that these biomarkers play an important role in stressor classification. These results support the fact that stress responses involve participants' vascular dynamics, neural stimulation and metabolism.

On the basis of the classification results, we expanded our analysis to the evaluation of state anxiety levels. We adopted a similar XGBoost

regression model and could predict state anxiety levels with a high confidence level of 98.7% and 98.1% coefficient of determination of scores from the STAI-Y (with a s.d. of 4 points or less[48]) (Fig. 4h and Supplementary Note 6). The relevance of each feature was evaluated using SHAP analysis as well (Fig. 4i,j). Through SHAP analysis, it was determined that GSR, pulse, Na^+, K^+ and lactate played the most important roles in predicting state anxiety levels. Note that SHAP values show the relative importance of each feature in the ML model. Additionally, given the intrinsic limitations of questionnaires, which can only characterize state anxiety levels in a given time period rather than continuous dynamic stress change, we analysed the stress response event as a whole to mimic questionnaire functionalities (Supplementary Note 3). In this circumstance, features were extracted from the stress region by taking mean signal changes from the moving average (MA) of sensor data rather than segmented at each timepoint, and a simple linear regression model was trained with fewer features selected
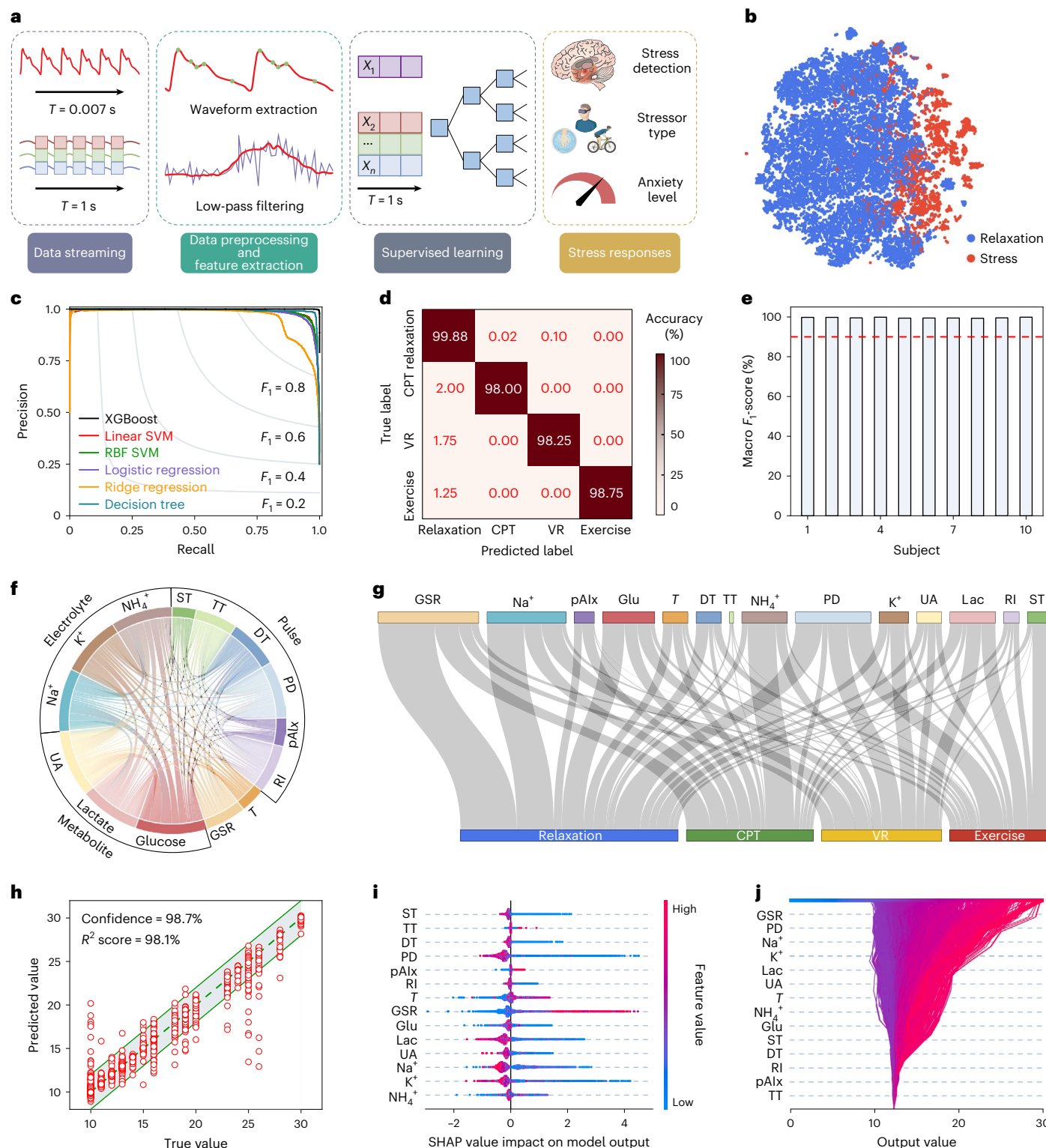
Fig. 4 | ML-powered stress response assessment. a, Schematics of the ML architecture for data preprocessing, feature extraction, supervised learning and evaluation. **b**, *t*-distributed stochastic neighbour embedding plot from the dataset recorded by the CARES, visually showing feature separation in a two-dimensional space. **c**, Precision–recall curve of different ML models for stressor classification. **d**, Confusion matrix displaying the classification accuracy for predicting each type of stressor in test set. **e**, The overall stress classification accuracy based on macro-averaged F_1-score for each subject. **f**, Chord diagram showing the relative correlation between different sensors. **g**, Sankey diagram of SHAP analysis depicting the relative contribution of different sensors to stressor classification. **h**, True versus ML-predicted state anxiety scores. Data are presented as ±2 state anxiety score buffer based on the potential error in the anxiety questionnaires. **i**, SHAP summary plot for state anxiety level evaluation based on the dataset collected by the CARES. Each axis plots the distribution of SHAP values of a given feature for each prediction instance. **j**, SHAP decision plot explaining how the ML model determines the state anxiety level using both physiological and biochemical features. DT, dicrotic peak time; PD, pulse duration; pAIx, peripheral augmentation index; RBF, radial basis function; RI, reflection index; ST, systolic time; TT, tidal peak time.

to correspond to questionnaire scores and prevent overfitting (Supplementary Fig. 40). With the reduced size of the dataset and analysing the overall sensor responses in the CARES, we performed a brute-force feature selection in each biomarker and found that combined physicochemical features outperformed those of physical and chemical sensors alone.

To realize convenient data collection for real-life applications, in addition to using flexible cables connecting the CARES patch with laboratory instruments (Supplementary Fig. 41), we further designed a fully integrated wearable CARES system with a flexible printed circuit board for multiplexed and multimodal signal processing as well as Bluetooth wireless communication (Supplementary Figs. 42–44). The wireless system was successfully used for on-body tests and validation of our CARES systems in the laboratory setting (Supplementary Fig. 45) and in real-life daily casual activities (Supplementary Fig. 46 and Supplementary Video 2). Our ML models obtained from the laboratory tests were able to accurately classify the types of stressors and state anxiety levels on the basis of the wirelessly collected sensor data in the laboratory (Supplementary Fig. 47) as well as real-life settings (Supplementary Fig. 48). We anticipate that for large-scale human trials, the CARES will surpass the current gold standards for stress response quantification and provide a highly robust stress response monitoring tool that is not reliant on subjective reporting with its potential for errors. In this regard, we envision a high potential for wearable multimodal physicochemical monitoring of dynamic stress response.

Conclusions

We have reported a CARES platform that performs multiplexed monitoring of key physiological signals, metabolites and electrolytes simultaneously during a prolonged operation. By applying analogous composite materials for stabilizing and conserving sensor interfaces, we developed a general approach to prepare stable and sensitive biochemical sensors including both enzymatic and ISE sensors, which offer long-term stability of more than 100 h of continuous operation with negligible sensor degradation. Continuous 24 h monitoring of prolonged daily activities was also obtained. Real-time multimodal data for stress responses were generated from three different stressors using both biochemical and physiological signals. With the enhanced reliability of sensor readings, we showed that a state of stress versus relaxation, and state anxiety as a key psychological response to stress, can be classified and predicted through multimodal health profiles at the metabolic level, with the ability to detect and classify stressor types with an accuracy of more than 98.0% and evaluate state anxiety levels at a confidence level of 98.7%. By capturing a broader range of signals through more integrated biosensors, a more complete metabolic profile could be achieved for next-generation healthcare and human performance monitoring. Our CARES could be of use in the development of numerous practical wearable applications including intelligent healthcare and personalized medicine.

Methods

Materials
SEBS (Tuftec) was provided by the Asahi Kasei Corporation. UA, sodium tetraphenylborate and glutaraldehyde (25% aqueous solution) were purchased from Alfa Aesar. Agarose, carbachol, BSA, gold chloride trihydrate, hydrochloric acid, iron(III) chloride, potassium ferricyanide (III), potassium ferrocyanide (IV), PVC, polyvinyl butyral (PVB), DOS, 3,4-ethylenedioxythiophene, poly(sodium 4-styrenesulfonate), aniline, L-lactic acid, sodium ionophore X, sodium tetrakis[3,5-bis(trifluoromethyl) phenyl] borate, valinomycin, nonactin, tetrahydrofuran (THF), toluene, glucose oxidase from Aspergillus niger (216 U mg^{-1}) and uricase from Bacillus fastidiosus (15.6 U mg^{-1}) were purchased from Sigma-Aldrich. Methanol, ethanol, sodium chloride, potassium chloride, nickel chloride, urea, L-ascorbic acid, dextrose (D-glucose)

anhydrous and PBS were purchased from Thermo Fisher Scientific. Lactate oxidase (106 U mg^{-1}) was purchased from Toyobo Co. Medical tapes (M-tapes) were purchased from 3M (468 MP). Polyethylene terephthalate (PET) films (12 μm thick) were purchased from McMaster-Carr. PI (2611) was purchased from HD MicroSystems, Inc. PDMS (SYLGARD 184) was purchased from Dow Corning. PI film (12.5 μm) was purchased from DuPont. STAI questionnaire license was purchased from Mind Garden, Inc.

Fabrication and assembly of the CARES device
CARES patch fabrication. The fabrication process of the CARES is illustrated in Supplementary Figs. 2 and 3. PI was spin-coated on the silicon oxide wafer at a speed of 5,000 revolutions per minute (r.p.m.) for 30 s and then cured at 350 °C for 1 h with a ramping speed of 4 °C min^{-1}. The resulting PI substrate thickness is about 4 μm. For mass fabrication, 12.5 μm PI film was used for large-area patterning demonstration. The CARES patch was then patterned with sequential printing of silver (interconnects and pin connections, reference electrode, pulse sensor and GSR sensor), carbon (IP electrodes, counter electrode, temperature sensor, working electrodes for biosensors) and PI (encapsulation) using an inkjet printer (DMP-2850, Fujifilm). The CARES patch was then annealed at 250 °C for 1 h. A 1:12 mixture of curing agent to PDMS elastomer was prepared and stirred thoroughly for 10 min, after which the solution was spin-coated at a speed of 800 r.p.m. for 30 s directly onto the inkjet-printed bottom layer of the CARES patch, followed by curing at 60 °C for 1 h. The resulting PDMS thickness is about 120 μm. Both the bottom and top layers of the CARES patch were then laser patterned to define outlines and sweat outlets using a 50 W CO$_2$ laser cutter (Universal Laser System) with power 25%, speed 50% and pulse per inch (PPI) 1,000 in vector mode. The bottom layer was further cut to define IP reservoirs, sweat reservoirs and airgaps without cutting through the PI substrate, with optimized parameters of power 2%, speed 20%, PPI 500 in vector mode, twice. The PDMS layer was cleaned with ethanol and deionized water to remove debris, followed by 30 s of O$_2$ plasma surface treatment using Plasma Etch PE-25 (10 cm^3 min^{-1} O$_2$, 100 W, 150 mTorr) to clean its surface and promote surface adhesion. The entire CARES patch was then assembled by dry transferring the top layer onto the bottom layer using a PDMS stamp. Biosensors were prepared before microfluidics integration. Note that the sweat reservoir was predefined during fabrication of the 120-μm-thick PDMS middle layer of the CARES patch, which has dimensions of 17.15 mm^2 and therefore a reservoir volume of 2.06 μl. The small volume allows a fast refreshing rate and enables rapid detection of dynamic changes during human performance.

Microfluidics fabrication. The microfluidics layers were fabricated with a laser cutter, layer by layer, by patterning double-sided M-tape, PET and PDMS with IP gel reservoirs, gel electrolytes reservoirs, sweat inlets, flowing channels and outlets. The optimized laser parameters to cut M-tape were set to power 62%, speed 100%, PPI 500 in vector mode, twice; and the optimized parameters to cut PDMS were power 2%, speed 20%, PPI 500 in vector mode, twice, to minimize debris. The IP gel and gel electrolytes reservoirs were patterned by cutting through all microfluidics layers to define the gel area and establish a gel connection with the skin. The first microfluidics layer is a PDMS-based sweat channel layer, which was spin-coated on a PET petri dish and cured at 60 °C for 1 h. The PDMS layer was treated with O$_2$ plasma before laminating a thin layer of 12 μm PET, followed by laser-defining sweat inlets. Then the third layer of double-sided M-tape was patterned and aligned onto PET, which contacts the skin and forms the sweat accumulation layer. After attaching the microfluidics module to the CARES patch, the system was further encapsulated with PDMS backings to avoid potential sweat contact and leakage. The device was connected with a flexible printed circuit connector for further characterization.

IP gel fabrication. Both the anode and cathode of IP gel were prepared by mixing agarose (3% w/w) into deionized water and then heated to 250 °C under constant stirring until the solution became homogenous. The solution was then cooled to 165 °C, during which 1% w/w carbachol and 1% w/w NaCl were added to the anode and cathode solutions, respectively, and mixed thoroughly. The solution was further cooled and poured into the IP gel reservoirs: 41.95 mm² for the anode and 28.19 mm² for the cathode, respectively. Together with the IP gel, electrolyte gel (SignaGel, Parker Laboratories, Inc.) was casted onto the GSR electrodes before the CARES device was placed on human subjects.

Biosensor preparation and characterization

Enzymatic sensor preparation. An electrochemical workstation (CHI 760E, CH Instruments) was used to prepare enzymatic biosensors. Pulsed voltammetry from −0.9 to 0.9 V (3,000 cycles total) in 50 mM HAuCl₄ was used to deposit gold nanoparticles on the carbon electrode at a signal frequency of 50 Hz, to increase surface area and enhance sensitivity. A thin PB transducer layer was deposited by applying cyclic voltammetry for two cycles for glucose and UA and four cycles for lactate (from −0.2 to 0.6 V with a scan rate of 50 mV s⁻¹) in a fresh solution consisting of 2.5 mM FeCl₃, 2.5 mM K₃Fe(CN)₆, 100 mM KCl and 100 mM HCl. The electrodes were then deposited with a NiHCF protection layer by applying cyclic voltammetry for 50 cycles (from 0 to 0.8 V with a scan rate of 100 mV s⁻¹) in a fresh solution containing 0.5 mM NiCl₂, 0.5 mM K₃Fe(CN)₆, 100 mM KCl and 100 mM HCl. The electrodes were then dried before drop-casting with an enzyme cocktail. For all three amperometric enzymatic sensors, the enzyme cocktails were prepared as follows: BSA (1% w/w), 2.5% glutaraldehyde (2% v/v) and 10 mg ml⁻¹ enzyme (4% v/v) were mixed in 1 ml PBS. Then 0.5 μl of enzyme cocktail was drop-casted onto each enzymatic sensor electrode surface and dried overnight at 4 °C. For the lactate sensor, a limit-diffusion membrane was further drop-casted by applying 0.5 μl of a solution containing 17 mg PVC and 65 mg DOS in 660 μl THF.

Reference electrode preparation. To prepare the shared reference electrode, 10 μl of 0.1 M FeCl₃ solution was drop-casted onto the Ag surface for 20 s and rinsed with deionized water. Then 1.5 μl PVB reference cocktail was applied on the Ag/AgCl surface by dissolving 79.1 mg PVB and 50 mg NaCl into 1 ml methanol and left to dry overnight.

ISE sensor preparation. The Na⁺ selective cocktail was prepared as follows: 1 mg Na ionophore X, 0.55 mg sodium tetrakis[3,5-bis(trifluoromethyl) phenyl] borate, 30 mg PVC, 30 mg SEBS and 65 mg DOS were dissolved in 660 μl THF. The K⁺ selective cocktail was prepared as follows: 2 mg valinomycin, 0.5 mg sodium tetraphenylborate, 30 mg PVC, 25 mg SEBS and 70 mg DOS were dissolved in 350 μl THF. The NH₄⁺ selective cocktail was prepared as follows: 1 mg nonactin, 30 mg PVC, 30 mg SEBS and 65 mg DOS were dissolved in 660 μl THF. The inkjet carbon electrode was activated in 0.5 M HCl with cyclic voltammetry scans of ten cycles (−0.1 to 0.9 V with a scan rate of 100 mV s⁻¹). The electrodes were baked in a vacuum oven at 120 °C for 1 h to remove moisture. Then 2 μl Na⁺ selective cocktail, 2 μl K⁺ selective cocktail and 2 μl NH₄⁺ selective cocktail were drop-casted onto the carbon electrode and dried overnight.

In vitro sensor characterization. To obtain the best performance for long-term continuous measurements, all sensors were placed in a buffered solution containing 100 μM glucose, 5 mM lactate, 25 μM UA, 40 mM NaCl, 8 mM KCl and 2 mM NH₄Cl for 30 min to minimize potential drift. All the in vitro biosensor characterizations were performed with cyclic voltammetry and amperometry through a multichannel electrochemical workstation (CHI 1430, CH Instruments). For in vitro enzymatic sensor characterizations, analyte solutions were prepared in PBS, with glucose ranging from 0 to 100 μM, lactate ranging from 0 to 20 mM and UA ranging from 0 to 100 μM. For in vitro ISE sensor characterizations, analyte solutions were prepared in deionized water, with NaCl ranging from 10 to 160 mM, KCl ranging from 2 to 32 mM and NH₄Cl ranging from 0.5 to 8 mM. The enzymatic sensors were characterized chronoamperometrically at a potential of 0 V, and the ISE sensors were characterized using open circuit potential measurement. Both potentiometric and chronoamperometric responses were set to a 1 s sampling interval, except for long-term monitoring, where the sampling interval was set to 10 s to minimize data overload. To test the pH influence on PB−NiHCF-based enzymatic biosensors, McIlvaine buffer solutions were prepared and calibrated containing 0−100 μM H₂O₂. Temperature influence characterizations were carried out on a ceramic hot plate (Thermo Fisher Scientific).

To characterize the stability of the PB and PB−NiHCF electrodes, dissolved Fe²⁺ concentrations were determined by inductively coupled plasma−mass spectrometry using an Agilent 8800. The sample introduction system consisted of a micromist nebulizer, Scott-type spray chamber and fixed-injector quartz torch. A guard electrode was used, and the plasma was operated at 1,500 W. All elements were measured in Helium tandem mass spectrometry mode.

Materials characterization

The morphology of materials was characterized by field-emission scanning electron microscopy (Nova 600). Cross-sectional lamella was prepared by standard focus ion beam cutting (Nova 600). The STEM characterizations and EDS analyses were performed using a JEOL JEM-ARM300CF S/STEM system (300 keV).

Physical sensor characterization

For in vitro temperature and GSR sensor characterizations, an amperometric method was used with an applied voltage of 1 V using a dual-channel electrochemical workstation (CHI 760E).

For in vitro pulse sensor characterizations, a parameter analyser (Keithley 4200A-SCS) was applied to record the fast-changing capacitive signals at a sampling frequency of around 137 Hz. The influence of mechanical deformation on physical sensor performance was investigated through pressing-releasing for 5,000 cycles using a Mark-10 force gauge. The influence of humidity was investigated by immersing the subject hand with the CARES in a customized glove box with a humidity gauge.

Microfluidics evaluation

On-body flow tests were conducted to evaluate the sweat flow of dual-reservoir designs. An assembled microfluidic patch predeposited with black dye in the sweat reservoir was attached to a subject's forearm, followed by in situ sweat induction using IP .

Experimental flow tests were also conducted to evaluate the dynamic response of sensors using a syringe pump (78−01001, Thermo Fisher Scientific). Different fluids were injected into the pre-assembled CARES device with a varying flow rate of 1−4 μl min⁻¹ (Supplementary Fig. 22).

On-body evaluation of CARES for long-term continuous monitoring

Subject recruitment. The validation and evaluation of the CARES device were performed on healthy human subjects in compliance with the protocols (19−0892 and 19−0895) approved by the Institutional Review Board at the California Institute of Technology (Caltech). Participating subjects were recruited from the Caltech campus and neighbouring communities through advertisement by posted notices, word of mouth and email distribution. Ten healthy subjects (eight males and two females, age range 23−38 years) were included in this study. The participants were healthy, without anxiety nor depression issues. All subjects gave written informed consent before participation in the study. The study was fully voluntary, and no compensation was given.

On-body protocols. The CARES was mounted on the subject's wrist after skin cleaning with alcohol wipes. Participants were requested to refrain from meals, alcohol, caffeine and exercise within 3 h before the tests. The CARES was sealed in PDMS, leaving output pins exposed with an M-tape backing as support for wire connections. We further designed a plug-and-play input–output to connect with the flexible flat cable (Supplementary Fig. 41). A 50 μA current was implemented on both pairs of IP electrodes for 5 min simultaneously for sweat induction. The data were collected with an eight-channel multiplexer (CHI Instrument 1430) and a Keithley 4200A-SCS parameter analyser. A wireless wearable CARES system was also developed for convenient data collection in real-life settings.

Long-term multimodal sensor evaluation during daily activities. Continuous monitoring of 24 h of physiological and biochemical signals was recorded using the CARES device. Five-minute periodical IP sweat induction was performed at 7 a.m., 9:30 a.m., 12:30 p.m., 4 p.m., 7 p.m., 11 p.m., 1:30 a.m. and 4:30 a.m. The physiological data were collected continuously, and data from the biosensors were collected 10 min after IP.

Questionnaire for state anxiety evaluation. STAI-Y is a self-evaluation questionnaire that consists of two forms (Y-1 and Y-2) to measure state and trait anxiety, respectively. It has a high internal consistency coefficient of 0.91–0.93 for college students and working adults[48]. In our study, we used short form Y-1, which measures state anxiety, as a key psychological response to stress. This measure can be proctored during real-time experiments without major intervention during the stress event. One challenge for quantifying stress is the subjective nature of the questionnaire, which inherently leads to small fluctuations of various stress points, with a s.d. of more than four points in most cases[48]. In our study, we take ±2 points as the confidence interval buffer for state anxiety level evaluation.

Stressor 1: CPT. The participants were asked to wear the CARES and relax for 10 min after IP sweat induction, during which no sensor signals were collected. After the relaxing stage, the physical sensors and biosensors simultaneously started monitoring baseline vital and molecular data. The STAI-Y questionnaire was administered to assess state anxiety levels during this relaxed baseline state. Subjects were asked to relaxation for another 1,000 s, after which a 3 min CPT was conducted. Subjects were asked to immerse their other hand without the CARES device up to the forearm into a tank containing iced water (0 °C) for 3 min. Another STAI-Y questionnaire was then given to evaluate state anxiety levels, and subjects were asked to finish within 20 s. Afterwards, subjects were instructed to remove the hand from the iced water and recover in ambient air. Continuous monitoring of multimodal physiological and biochemical data was performed throughout the stress challenge and recovery stage until 1,000 s after the CPT was finished. The subjects were seated during the whole procedure.

Stressor 2: VR test. The sensor data recording process was the same as the aforementioned, except that subjects were asked to play a VR game (Beat Saber) while wearing a VR headset (Oculus Quest 2, Meta). The game was set to one-handed mode with expert difficulty, and the game screen was projected onto a monitor. Subjects were strongly encouraged verbally and asked to compete with other participants' record scores so that mixed physical and psychological stress could be stimulated. The STAI-Y questionnaire was used to assess state anxiety levels.

Stressor 3: exercise. For exercise-induced stress, the sensor data recording process was the same as the aforementioned. Subjects performed maximum-load cycling (>70 r.p.m.) on a stationary exercise bike (Kettler Axos Cycle M-LA) for 3 min or until fatigue, during which strong verbal encouragement was given. The STAI-Y questionnaire was used to assess state anxiety levels.

Data collection in real-life activities. Subjects was asked to perform indoor activities, including relaxation on the phone, playing a long-term VR game (Superhot VR) while wearing a VR headset and reading journal papers. Subjects then performed outdoor activities, including running and walking recovery. The STAI-Y questionnaire was used to assess state anxiety levels during each activity.

ML pipeline for stress assessment

Data preprocessing and feature extraction. Although all the multimodal sensor signals were monitored in real time, data preprocessing was performed asynchronously to extract features. A pulse feature extraction algorithm was developed because of its unique peripheral pulse sampling frequency of $T = 0.007$ s. To match the other sensors' sampling frequency of $T = 1$ s, each pulse waveform was autonomously analysed through our pulse analysis algorithm, and a floor function was used afterwards to select the closest pulse feature within each time interval. Signals from the biochemical sensors were manually shifted by 300 s to align with physical signals due to natural sweat delay; heart rate data in figure plots were extracted from the pulse features and smoothed by the MA of 100 s to show the trends more clearly. The time stamp when each subject expressed stress was recorded, and manual data labelling was performed. To minimize variations from intersubject responses, all features were normalized before the ML pipeline with regard to each subject during each stress test, to generalize the model among the population. After data collection and analysis, the training and testing datasets were shuffled and divided 8:2, respectively, and data points were randomly selected using an equal representation of each class. The ML model was developed to link biological and chemical features to stress detection, stress types and state anxiety levels from questionnaire scores.

Model selection for stress classification. All training models were built using Python (v.3.8) based on the data collected from ten subjects facing three different stressors, with a set of 60,000 s of CARES recordings. Segmentation of the sensor signals was done using a sliding window with a sampling interval of 1 s, given each stress type representation. Several ML models were evaluated according to their precision–recall curves and F_1-scores, including linear and radial basis function SVMs, logistic and ridge regression, conventional decision trees and the gradient-boosted decision tree XGBoost model. The trained XGBoost model outperformed typical ML models for both stress detection and stress type classification.

Model selection for stress regression. The ML algorithms were developed on a password-protected local computer with individual graphics processing unit module Nvidia 3080. The training models were built as mentioned earlier, except that the kernel was changed to a regressor instead of a classifier. For overall stress level evaluations, on the other hand, features were extracted from stress regions by taking average signal changes from the MA of sensors rather than segmented at each timepoint, and simpler ML models such as linear regression and SVM were evaluated because of the reduced size of the datasets, to prevent overfitting. A brute-force examination of features was performed to compare the contributions of physicochemical biomarkers.

Reporting summary

Further information on the research design is available in the Nature Portfolio Reporting Summary linked to this article.

Data availability

The multimodal data collected by the CARES from human subjects is available at https://github.com/CARES-eskin/StressData. All other

data that support the findings of this study are available from the corresponding author on reasonable request.

References

1. Kivimäki, M., Bartolomucci, A. & Kawachi, I. The multiple roles of life stress in metabolic disorders. *Nat. Rev. Endocrinol.* **19**, 10–27 (2022).
2. Schneiderman, N., Ironson, G. & Siegel, S. D. Stress and health: psychological, behavioral, and biological determinants. *Annu. Rev. Clin. Psychol.* **1**, 607–628 (2005).
3. Kumar, A., Rinwa, P., Kaur, G. & Machawal, L. Stress: neurobiology, consequences and management. *J. Pharm. Bioallied Sci.* **5**, 91–97 (2013).
4. Podsakoff, N. P., Freiburger, K. J., Podsakoff, P. M. & Rosen, C. C. Laying the foundation for the challenge–hindrance stressor framework 2.0. *Annu. Rev. Organ. Psychol. Organ. Behav.* **10**, 165–199 (2023).
5. Pfefferbaum, B. & North, C. S. Mental health and the COVID-19 pandemic. *N. Engl. J. Med.* **383**, 510–512 (2020).
6. Santomauro, D. F. et al. Global prevalence and burden of depressive and anxiety disorders in 204 countries and territories in 2020 due to the COVID-19 pandemic. *Lancet* **398**, 1700–1712 (2021).
7. Gutshall, C. L., Hampton, D. P., Sebetan, I. M., Stein, P. C. & Broxtermann, T. J. The effects of occupational stress on cognitive performance in police officers. *Police Pract. Res.* **18**, 463–477 (2017).
8. Tomporowski, P. D. Effects of acute bouts of exercise on cognition. *Acta Psychol.* **112**, 297–324 (2003).
9. Martin, K. et al. The impact of environmental stress on cognitive performance: a systematic review. *Hum. Factors* **61**, 1205–1246 (2019).
10. Robinson, S. J., Leach, J., Owen-Lynch, P. J. & Sünram-Lea, S. I. Stress reactivity and cognitive performance in a simulated firefighting emergency. *Aviat. Space Environ. Med.* **84**, 592–599 (2013).
11. Haines, M. M., Stansfeld, S. A., Job, R. F. S., Berglund, B. & Head, J. Chronic aircraft noise exposure, stress responses, mental health and cognitive performance in school children. *Psychol. Med.* **31**, 265–277 (2001).
12. Kulshreshtha, A. et al. Association of stress with cognitive function among older black and white US adults. *JAMA Netw. Open* **6**, e231860 (2023).
13. Epel, E. S. et al. More than a feeling: a unified view of stress measurement for population science. *Front. Neuroendocrinol.* **49**, 146–169 (2018).
14. Thapar, A., Eyre, O., Patel, V. & Brent, D. Depression in young people. *Lancet* **400**, 617–631 (2022).
15. Topol, E. *Deep Medicine: How Artificial Intelligence Can Make Healthcare Human Again* (Basic Books, 2019).
16. Herrman, H. et al. Time for united action on depression: a Lancet–World Psychiatric Association Commission. *Lancet* **399**, 957–1022 (2022).
17. Drew, D. A. et al. Rapid implementation of mobile technology for real-time epidemiology of COVID-19. *Science* **368**, 1362–1367 (2020).
18. Charmandari, E., Tsigos, C. & Chrousos, G. Endocrinology of the stress response. *Annu. Rev. Physiol.* **67**, 259–284 (2005).
19. Dolan, R. J. Emotion, cognition, and behavior. *Science* **298**, 1191–1194 (2002).
20. Harker, M. Psychological sweating: a systematic review focused on aetiology and cutaneous response. *Skin Pharmacol. Physiol.* **26**, 92–100 (2013).
21. Axelrod, J. & Reisine, T. D. Stress hormones: their interaction and regulation. *Science* **224**, 452–459 (1984).
22. Acosta, J. N., Falcone, G. J., Rajpurkar, P. & Topol, E. J. Multimodal biomedical AI. *Nat. Med.* **28**, 1773–1784 (2022).
23. Buergel, T. et al. Metabolomic profiles predict individual multidisease outcomes. *Nat. Med.* **28**, 2309–2320 (2022).
24. Ates, H. C. et al. End-to-end design of wearable sensors. *Nat. Rev. Mater.* **7**, 887–907 (2022).
25. Wang, C. et al. Bioadhesive ultrasound for long-term continuous imaging of diverse organs. *Science* **377**, 517–523 (2022).
26. Kim, D.-H. et al. Epidermal electronics. *Science* **333**, 838–843 (2011).
27. Xu, C., Yang, Y. & Gao, W. Skin-interfaced sensors in digital medicine: from materials to applications. *Matter* **2**, 1414–1445 (2020).
28. Niu, S. et al. A wireless body area sensor network based on stretchable passive tags. *Nat. Electron.* **2**, 361–368 (2019).
29. Gao, W. et al. Fully integrated wearable sensor arrays for multiplexed *in situ* perspiration analysis. *Nature* **529**, 509–514 (2016).
30. Wang, M. et al. A wearable electrochemical biosensor for the monitoring of metabolites and nutrients. *Nat. Biomed. Eng.* **6**, 1225–1235 (2022).
31. Kim, J., Campbell, A. S., de Ávila, B. E.-F. & Wang, J. Wearable biosensors for healthcare monitoring. *Nat. Biotechnol.* **37**, 389–406 (2019).
32. Ray, T. R. et al. Bio-integrated wearable systems: a comprehensive review. *Chem. Rev.* **119**, 5461–5533 (2019).
33. Chesnut, M. et al. Stress markers for mental states and biotypes of depression and anxiety: a scoping review and preliminary illustrative analysis. *Chronic Stress* **5**, 24705470211000338 (2021).
34. Xu, S., Kim, J., Walter, J. R., Ghaffari, R. & Rogers, J. A. Translational gaps and opportunities for medical wearables in digital health. *Sci. Transl. Med.* **14**, eabn6036 (2022).
35. Torrente-Rodríguez, R. M. et al. Investigation of cortisol dynamics in human sweat using a graphene-based wireless mHealth system. *Matter* **2**, 921–937 (2020).
36. Wang, B. et al. Wearable aptamer-field-effect transistor sensing system for noninvasive cortisol monitoring. *Sci. Adv.* **8**, eabk0967 (2022).
37. Sheibani, S. et al. Extended gate field-effect-transistor for sensing cortisol stress hormone. *Commun. Mater.* **2**, 10 (2021).
38. Simmers, P., Li, S. K., Kasting, G. & Heikenfeld, J. Prolonged and localized sweat stimulation by iontophoretic delivery of the slowly-metabolized cholinergic agent carbachol. *J. Dermatol. Sci.* **89**, 40–51 (2018).
39. Sancini, A. & Tomei, F. Work related stress and blood glucose levels. *Ann. Ig.* **29**, 123–133 (2017).
40. Hermann, R., Lay, D., Wahl, P., Roth, W. T. & Petrowski, K. Effects of psychosocial and physical stress on lactate and anxiety levels. *Stress* **22**, 664–669 (2019).
41. Kubera, B. et al. Rise in plasma lactate concentrations with psychosocial stress: a possible sign of cerebral energy demand. *Obes. Facts* **5**, 384–392 (2012).
42. Klous, L., de Ruiter, C. J., Scherrer, S., Gerrett, N. & Daanen, H. A. M. The (in)dependency of blood and sweat sodium, chloride, potassium, ammonia, lactate and glucose concentrations during submaximal exercise. *Eur. J. Appl. Physiol.* **121**, 803–816 (2021).
43. Goodman, A. M. et al. The hippocampal response to psychosocial stress varies with salivary uric acid level. *Neuroscience* **339**, 396–401 (2016).
44. Nyein, H. Y. Y. et al. A wearable electrochemical platform for noninvasive simultaneous monitoring of Ca^{2+} and pH. *ACS Nano* **10**, 7216–7224 (2016).
45. Lin, S. et al. Wearable microneedle-based electrochemical aptamer biosensing for precision dosing of drugs with narrow therapeutic windows. *Sci. Adv.* **8**, eabq4539 (2022).

46. Tu, J. et al. A wireless patch for the monitoring of C-reactive protein in sweat. *Nat. Biomed. Eng.* **7**, 1293–1306 (2023).

47. Shao, Y., Ying, Y. & Ping, J. Recent advances in solid-contact ion-selective electrodes: functional materials, transduction mechanisms, and development trends. *Chem. Soc. Rev.* **49**, 4405–4465 (2020).

48. Spielberger, C. D., Gorsuch, R. L., Lushene, R. E., Vagg, P. R. & Jacobs, G. A. (eds) *Manual for the State-trait Anxiety Inventory (STAI Form Y)* (Consulting Psychologists Press, 1983).

49. Frank, S. M. & Raja, S. N. Reflex cutaneous vasoconstriction during cold pressor test is mediated through α-adrenoceptors. *Clin. Auton. Res.* **4**, 257–261 (1994).

50. Schwabe, L., Haddad, L. & Schachinger, H. HPA axis activation by a socially evaluated cold-pressor test. *Psychoneuroendocrinology* **33**, 890–895 (2008).

51. Khambam, S. K. R., Naidu, M. U. R., Rani, P. U. & Rao, T. R. K. Effect of cold stimulation-induced pain on pharmacodynamic responses in healthy human volunteers. *Int. J. Nutr. Pharmacol. Neurol. Dis.* **2**, 26 (2012).

52. Buono, M. J., Lee, N. V. L. & Miller, P. W. The relationship between exercise intensity and the sweat lactate excretion rate. *J. Physiol. Sci.* **60**, 103–107 (2010).

53. Maaten van der, L. & Hinton, G. Visualizing data using t-SNE. *J. Mach. Learn. Res.* **9**, 2579–2605 (2008).

54. Hay, E. L. & Diehl, M. Reactivity to daily stressors in adulthood: the importance of stressor type in characterizing risk factors. *Psychol. Aging* **25**, 118–131 (2010).

55. Crestani, C. C. Emotional stress and cardiovascular complications in animal models: a review of the influence of stress type. *Front. Physiol.* **7**, 251 (2016).

56. Pow, J., Lee-Baggley, D. & DeLongis, A. Threats to communion and agency mediate associations between stressor type and daily coping. *Anxiety Stress Coping* **29**, 660–672 (2016).

57. Scheid, T. L. & Brown, T. N. (eds) *Handbook for the Study of Mental Health: Social Contexts, Theories, and Systems*. (Cambridge Univ. Press, 2009); https://doi.org/10.1017/CBO9780511984945

Acknowledgements

Author contributions

W.G. and C.X. conceived the project. C.X. led the sensors and CARES platform development. C.X., Y.S. and J.R.S. led the platform characterization and human studies. S.A.S. and J.L. contributed to the data processing and feature extraction. H.Y.Y.N. contributed to sensor development. Y.Y., R.Y.T. and A.L. contributed to sensor characterization and testing. W.H. and J.M. contributed to wireless system development. T.K.H. and J.A.S. contributed to the human study design. W.G., C.X., Y.S., J.R.S. and S.A.S. cowrote the paper. All authors contributed to the data analysis and provided feedback on the manuscript.

Competing interests

The authors declare no competing interests.

Additional information

Supplementary information The online version contains supplementary material available at https://doi.org/10.1038/s41928-023-01116-6.

Correspondence and requests for materials should be addressed to Wei Gao.

Peer review information *Nature Electronics* thanks Sihong Wang and the other, anonymous, reviewer(s) for their contribution to the peer review of this work.

Reprints and permissions information is available at www.nature.com/reprints.

Publisher's note Springer Nature remains neutral with regard to jurisdictional claims in published maps and institutional affiliations.